Research Article

Contrast Enhancement of Brain Aneurysms on High-Resolution Vessel Wall Imaging [HR-VWI] Correlates with the Presence of Microbleeds

Jorge A Roa MD[1], Mario Zanaty[2], Anthony J Piscopo BS[2], Timothy W Morris BS[2], Ryan Sabotin BS[3], Daizo Ishii MD[2], Alberto Varon MD[3], Ashrita Raghuram[3], Yongjun Lu PhD[2], Edgar A Samaniego MD, MS[2,3,4], David M Hasan MD[2*]

[1]Department of Neurosurgery, Icahn School of Medicine at Mount Sinai, New York, NY, USA

[2]Department of Neurosurgery, University of Iowa Hospitals and Clinics, Iowa City, IA, USA

[3]Department of Neurology, University of Iowa Hospitals and Clinics, Iowa City, IA, USA

[4]Department of Radiology, University of Iowa Hospitals and Clinics, Iowa City, IA, USA

[*]**Corresponding Author:** David M Hasan, MD, Section Chief of Vascular Neurosurgery, Professor of Neurosurgery, Otolaryngology, and Biomedical Engineering, University of Iowa Hospitals and Clinics, 200 Hawkins Drive, Iowa City, IA, USA, Tel: 319-400-9455; E-mail: david-hasan@uiowa.edu

Received: 08 February 2021; **Accepted:** 17 February 2021; **Published:** 22 February 2021

Citation: Jorge A Roa, Mario Zanaty, Anthony J Piscopo, Timothy W Morris, Ryan Sabotin, Daizo Ishii, Alberto Varon, Ashrita Raghuram, Yongjun Lu, Edgar A Samaniego, David M Hasan. Optical Coherence Tomography: A Contemporary Realism in Stent Fracture. Cardiology and Cardiovascular Medicine 5 (2021): 162-171.

Abstract

Background: Wall enhancement of unruptured intracranial aneurysms (UIAs) on high-resolution vessel wall imaging (HR-VWI) has been applied as a surrogate of inflammation. MR-quantitative susceptibility mapping (QSM) can identify microbleeds (MBs) at the interface between aneurysm wall and brain tissue preceding subarachnoid hemorrhage.

Objective: To assess the correlation between HR-VWI and QSM findings and define an optimal cut-off for aneurysm wall enhancement based on the presence of MBs.

Methods: Patients with UIAs prospectively underwent QSM and HR-VWI. UIAs were deemed unstable when MBs were identified on QSM. The contrast enhancement ratio between maximal signal

intensity values measured in the aneurysmal wall and the pituitary stalk (CR_{stalk}) on T1 post-contrast images was calculated. Multiple *t*-tests were computed to assess the correlation between morphological variables, PHASES scores, CR_{stalk}, and presence of MBs. A ROC curve was plotted to determine the best CR_{stalk} cutoff to differentiate stable from unstable UIAs.

Results: A total of 81 UIAs were analyzed: 71 stable (MBs absent) and 10 unstable (MBs present). Unstable UIAs were larger (8.4 ± 5.5 mm vs 5.5 ± 2.3 mm, P=0.007), showed higher CR_{stalk} (0.6 ± 0.2 vs 0.5 ± 0.1, P=0.05), and scored higher on PHASES (6.9 ± 3.5 vs 4.8 ± 2.6, P=0.02). ROC curve analysis demonstrated the best CR_{stalk} cut-off to discriminate between UIAs with and without MBs was ≥ 0.55 (82% sensitivity, 67% specificity).

Conclusion: There is a strong positive association between aneurysmal wall enhancement and presence of MBs. CR_{stalk} ≥ 0.55 may be used as a surrogate biomarker of aneurysmal instability in clinical practice.

Keywords: Contrast enhancement; Intracranial aneurysm; Rupture risk; Microbleeds; HR-VWI; QSM; MRI

1. Introduction

High-resolution vessel wall imaging (HR-VWI) has recently surfaced as a potential tool to assess the rupture risk of unruptured intracranial aneurysms (UIAs). A first report by Matouk et al. retrospectively applied HR-VWI in 5 patients with multiple intracranial aneurysms who had suffered subarachnoid hemorrhage (SAH). They demonstrated that avid aneurysm wall enhancement (AWE) was always detectable in the culprit ruptured aneurysms [1]. Further studies have associated AWE with clinical features of instability, including larger size [2-4], location in the posterior communicating or posterior circulation arteries [2], and irregular shape [5, 6]. Moreover, histopathological analyses have demonstrated that avid AWE correlates with increased levels of inflammation in the aneurysm wall, such as lymphocyte infiltration [7], active macrophage infiltration [8, 9], higher myeloperoxidase activity [10], decreased elastin [9], neovascularization [11], and vasa vasorum disease [8, 10]. All of these studies have suggested that AWE of UIAs may be used as a biomarker of instability. To date, two prospective studies have demonstrated a positive association between AWE and aneurysm instability over time. Vergouwen et al. analyzed 57 patients with 65 UIAs. After a median follow-up of 27 months, 4/19 UIAs with AWE became unstable: 2 grew and 2 ruptured. On the other hand, all 46 UIAs without AWE remained stable throughout the study [12]. Gariel et al. analyzed 129 patients with 145 UIAs. Over a 2-year period, 12 UIAs grew: 8 showed increased AWE during follow-up and 4 had preexisting AWE visualized at baseline. In the remaining 133 stable UIAs, no AWE modifications were found [13].

Quantitative-Susceptibility Mapping (QSM) is a distinct MRI sequence specifically developed to quantify tissue magnetic susceptibility [14]. QSM is widely used to quantitatively measure the non-heme iron content of different brain structures in pathologies such as cavernous malformations, multiple sclerosis, and Alzheimer's disease. Based on this premise, Nakagawa et al. used QSM to assess presence of microbleeds (MBs) in the wall of 20 UIAs harbored by 16 patients. Clinical presentation in 4 of the patients (two of whom had 2 aneurysms each) met the typical definition of sentinel headache,

whereas the remaining 12 patients had migraine headache. Interestingly, QSM analysis was positive for MBs in all 4 patients with sentinel headache, allowing timely identification of unstable UIAs, prompt endovascular treatment, and prevention of SAH. In this study, we applied QSM analysis as the gold standard to define aneurysm instability and compared degree of AWE among UIAs with MBs (unstable) and without MBs (stable).

2. Methods

2.1 Patient Selection and Study Design

After institutional review board approval, patients with UIAs underwent 3T HR-VWI at diagnosis. Patients were recruited from January 2015 to May 2020. UIAs with non-saccular morphology (i.e. fusiform, blister-like) were excluded. Cavernous aneurysms were also excluded due to artifact of the cavernous sinus on T1-post contrast images. Additionally, due to limited spatial resolution of 3T MRI, UIAs <2 mm in size were also excluded. Demographic and clinical information necessary to calculate the scores was obtained from electronic medical records.

2.2 Imaging Acquisition

Images were routinely acquired with a 3T Siemens MRI scanner (Siemens MAGNETOM Skyra, Munich, Germany). The HR-VWI protocol included a 3D T1-weighted SPACE fast-spin-echo (FSE) and a 3D T2-weighted sequence. Five minutes after intravenous injection of 0.1 mmol/kg gadolinium-based contrast agent (Gadavist, Bayer Pharmaceuticals, Whippany, NJ), a post-contrast 3D T1-weighted SPACE FSE sequence and contrast-enhanced magnetic resonance angiography (CE-MRA) were obtained.

2.3 QSM Assessment

Quantitative Susceptibility Mapping (QSM) DICOM images were imported to Horos Medical Image Viewer (Nimble Co LLC, Annapolis, MD). Use of the Matlab toolbox was coupled with STI Suite, Laplacian-based phase processing on QSM files to produce tissue phase visualization [15]. Two blinded adjudicators, who are experienced vascular neurosurgeons, separately evaluated both the QSM and VWI images. In the case of disagreement between two adjudicators, a consensus was reached by discussion. The presence of MBs was evaluated by overlapping MRA images of the UIA with QSM images using 3D slicer, an open-source software platform [16]. Segmentation for MBs was performed using pixel-labeling methods with an optimal susceptibility threshold of 0.1 parts per million [17]. The regions with high-susceptibility in QSM images were strictly distinguished from the surrounding cerebral vasculature.

2.4 HR-VWI Assessment

All images were analyzed with Picture Archiving Communication System, version 12.1.6.1005 (Carestream Vue PACS, Rochester, NY). Our protocol for assessing aneurysmal wall enhancement on HR-VWI has been previously described [18, 19]. Briefly, the aneurysm was manually co-registered in both pre- and post-contrast T1-weighted sequences in three planes (axial, coronal, and sagittal). After six-fold magnification and auto-correction of viewer windowing, a 2D region of interest of the aneurysm wall was drawn at the level of maximal aneurysm diameter. CE-MRA and 3D T1 SPACE (pre-contrast) images were used as a reference to delineate the inner surface of the aneurysm wall.

Additionally, both 3D T2-weighted sequences and 3D T1-SPACE (post-contrast) images were used to

exclude surrounding artifacts such as cerebrospinal fluid, meninges, and veins. AWE was objectively quantified using the aneurysm-to-pituitary stalk contrast ratio (CR_{stalk}) as previously described [18]. Aneurysmal morphological characteristics (i.e. aspect ratio, size ratio, and irregular shape) were assessed with digital subtraction angiography (DSA), computed tomography angiography (CTA), or magnetic resonance angiography (MRA) as previously described [20]. Briefly, aspect ratio was calculated as the maximum perpendicular height divided by the average neck diameter. Size ratio was defined as the maximum aneurysm height divided by the average vessel diameter, which was obtained by measuring two representative vessel cross sections upstream of the aneurysm. Three different standardized clinical scores of aneurysm instability were calculated: (1) PHASES [21], (2) ELAPSS [22], and (3) UIATS [23].

Aneurysms were considered 'irregular' if blebs and/or daughter sacs were visualized on the aneurysmal surface. The quantification of aneurysm enhancement and morphological analysis was performed by two investigators blinded from clinical data.

2.5 Statistical Analysis

Continuous variables are presented as mean ± standard deviation (SD), and categorical variables are presented as frequency and percentage. Distributions of values for CR_{stalk} were tested for normality using the Kolmogorov-Smirnov method. For normally distributed values, Student's t-test was performed; for non-parametric distributions, Mann Whitney U-test was applied. Pearson's coefficient was used to assess for statistical correlation between PHASES, ELAPSS, UIATS, and aneurysmal wall enhancement as reflected by CR_{stalk}. A multivariable logistic regression was modelled to predict rupture risk using CR_{stalk} values. Variables with a p-value < 0.20 in the univariable analysis were included in the multivariable regression model. A 2-sided p-value < 0.05 was considered significant. All statistical analyses were performed with SPSS Statistics 25.0 (IBM, Armonk, New York) and GraphPad Prism version 8.1.2 (GraphPad Software, La Jolla, California).

3. Results

3.1 Patient Selection

One-hundred and twenty-three patients harboring 178 UIAs underwent HR-VWI. Of them, 97 UIAs (54%) were excluded: 54 due to QSM artifacts, 19 due to fusiform morphology, 9 due to size (<2 mm), 8 due to location in the cavernous segment of the internal carotid artery, and 7 due to poor HR-VWI quality. 81 unruptured IAs were analyzed: 71 stable (MBs absent) and 10 unstable (MBs present) (Figure 1).

3.2 Patients' Clinical and Demographic Characteristics

Baseline characteristics of the sample are presented in Table 1. Mean age was 63.1 ± 12.5 years, and 90% of aneurysms (73/81) were found in women. Among comorbidities, 73% of aneurysms were found in patients with hypertension, 32% in patients with hyperlipidemia, and 28% in patients who were current/past smokers. Mean aneurysmal size was 6.5 mm ± 3.9 mm, with 64% of aneurysms <7 mm. Most common location was the ICA/ACA (31%), followed by the MCA (22.2%), PCOM (14.8%), and BA tip (13.6%).

3.3 Unstable UIAs with MBs: Correlation with Clinical Risk Factors of Rupture

Our statistical analysis demonstrated significant differences between stable (MB-) and unstable

(MB+) UIAs in terms of (Table 1): (1) size > 7 mm (70% unstable vs 31% stable, p = 0.03), (2) mean SI (265.6 unstable vs 202.8 stable, p = 0.02), (3) PHASES ≥ 5 (80% unstable vs 46.5% stable, p = 0.04) and (4) CR_{stalk} (0.6 unstable vs 0.5 stable, p = 0.05).

3.4 Unstable UIAs with MBs: Correlation with CR_{stalk}

ROC curve analysis demonstrated that the best CR_{stalk} cut-off to discriminate between UIAs with and without MBs was ≥ 0.55 (82% sensitivity, 67% specificity) (Figure 2).

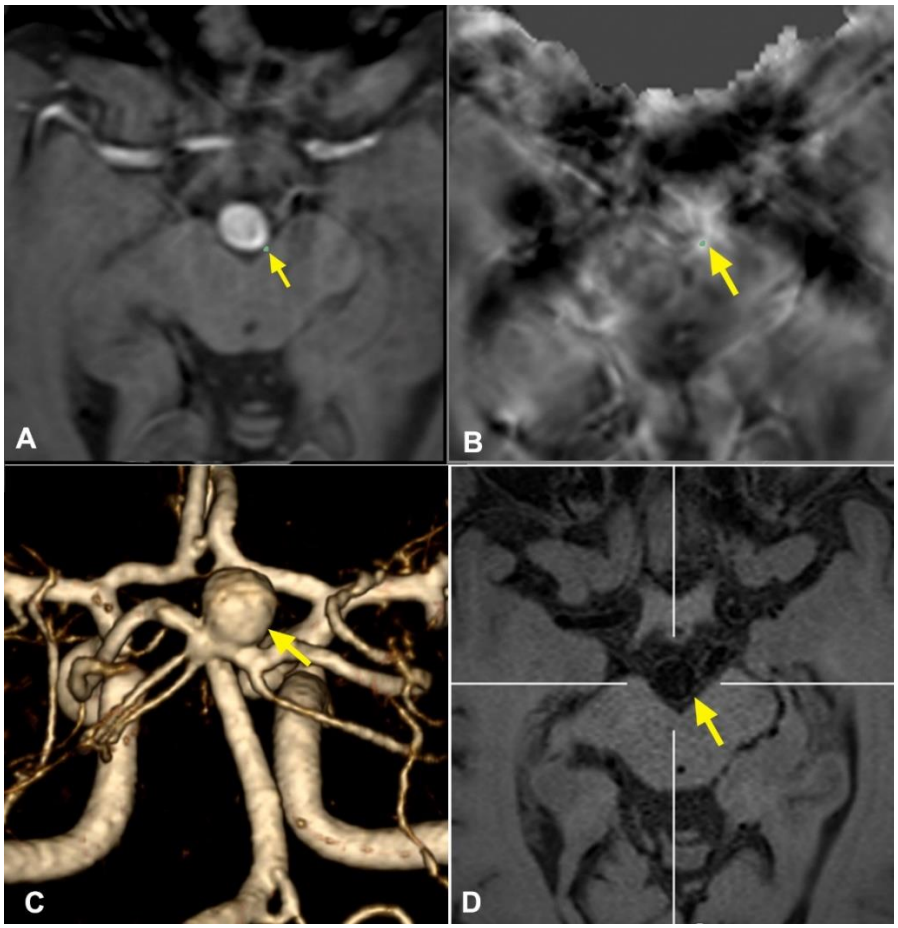

Figure 1: Representative case of a basilar tip aneurysm showing the methodology applied for HR-VWI and QSM analyses. (A) and (B): QSM sequences showing an area of microbleed in the left posterolateral aspect of the aneurysmal wall; (C): 3D MRA reconstruction of the aneurysm to characterize its morphology; (D): HR-VWI demonstrating an area of focal enhancement that corresponds with the microbleed.

Variable	**Overall UIAs (N=81)**	**Stable UIAs (MB-) (n=71)**	**Unstable UIAs (MB+) (n=10)**	***P***
Age (years, mean ± SD)	63.1 ± 12.5	62.2 ± 11.6	65.4 ± 11.5	0.41
Women (%)	73 (90.1)	64 (90.1)	9 (90)	0.98
Hypertension (%)	58 (71.6)	52 (73.2)	6 (60)	0.46

Diabetes (%)	11 (13.6)	11 (15.5)	0 (0)	0.34
Hyperlipidemia (%)	32 (39.5)	30 (42.3)	2 (20)	0.30
Smoking (%)	28 (34.6)	26 (36.6)	2 (20)	0.48
Family Hx SAH (%)	1 (1.2)	1 (1.4)	0 (0)	0.71
Size (in mm, mean ± SD)	6.5 ± 3.9	5.75 ± 2.9	8.7 ± 4.8	0.18
- < 7 mm (%)	52 (64.2)	49 (69)	3 (30)	**0.03**
- ≥ 7 mm (%)	29 (35.8)	22 (31)	7 (70)	
Location				0.37
- ICA/ACA (%)	25 (30.9)	21 (29.5)	4 (40)	
- ACOM (%)	9 (11.1)	9 (12.7)	0 (0)	
- MCA (%)	18 (22.2)	13 (18.3)	5 (50)	
- PCOM (%)	12 (14.8)	11 (15.5)	1 (10)	
- BA (%)	11 (13.6)	11 (15.5)	0 (0)	
- PICA/SCA/VA (%)	5 (6.2)	5 (7.1)	0 (0)	
Irregular shape (%)	53 (65.4)	47 (66.2)	6 (60)	0.73
Aspect ratio (mean ± SD)	1.95 ± 1.09	1.9 ± 0.86	2.12 ± 1.27	0.32
- < 1.6 (%)	38 (46.9)	34 (47.9)	4 (40)	0.74
- ≥ 1.6 (%)	43 (53.1)	37 (52.1)	6 (60)	
Size ratio (mean ± SD)	2.65 ± 1.39	2.6 ± 1.19	3.3 ± 1.58	0.51
- < 3 (%)	55 (67.9)	50 (70.4)	5 (50)	0.28
- ≥ 3 (%)	26 (32.1)	21 (29.6)	5 (50)	
Mean SI (mean ± SD)	228.3 ± 89.7	202.8 ± 71.5	265.6 ± 136.5	**0.02**
Maximal SI (mean ± SD)	387.3 ± 134.1	343.7 ± 116.9	422.7 ± 166.1	0.19
PHASES (mean ± SD)	4.85 ± 3.2	4.82 ± 2.6	6.9 ± 3.5	0.30
- < 5 (%)	40 (49.4)	38 (53.5)	2 (20)	**0.04**
- ≥ 5 (%)	41 (50.6)	33 (46.5)	8 (80)	
ELAPSS (mean ± SD)	16.8 ± 8.1	15.8 ± 7.2	20.8 ± 7	0.45
- < 17 (%)	38 (46.9)	37 (52.1)	1 (10)	**0.01**
- ≥ 17 (%)	43 (53.1)	34 (47.9)	9 (90)	
UIATS (mean ± SD)	1.01 ± 5.9	1.51 ± 6.03	0.70 ± 5.89	0.77
- < 1 (%)	36 (44.4)	30 (42.3)	6 (60)	0.29
- ≥ 1 (%)	45 (55.6)	41 (57.7)	4 (40)	
CR_{stalk} *(mean ± SD)*	0.56 ± 0.18	0.52 ± 0.16	0.62 ± 0.21	**0.05**
- < 0.60 (%)	58 (71.6)	52 (73.2)	6 (60)	0.46
- ≥ 0.60 (%)	23 (28.4)	19 (26.8)	4 (40)	

MB: microbleed; SAH: subarachnoid hemorrhage; SD: standard deviation; UIA: unruptured intracranial aneurysm.

Table 1: Baseline characteristics and univariate analysis between stable (MB-) and unstable (MB+) UIAs.

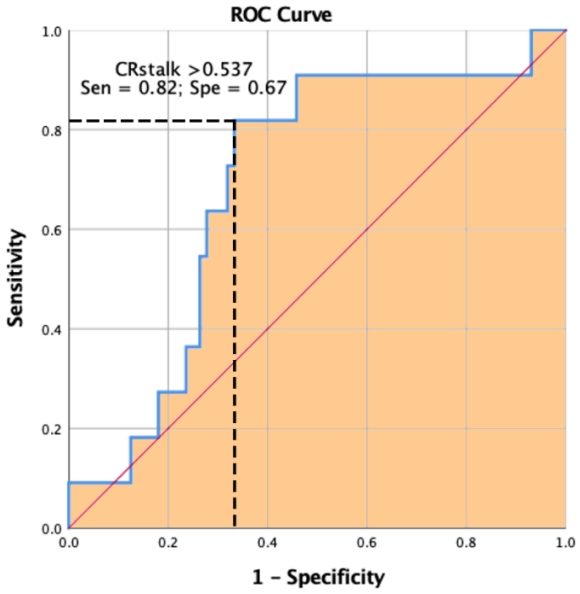

Figure 2: ROC curve depicting the best CR_{stalk} to predict presence of MBs in the aneurysmal wall.

4. Discussion

This HR-VWI study suggests that a CR_{stalk} greater than or equal to 0.55 can be used as an alternative biomarker of instability in addition to QSM. Positive QSM analysis strongly suggests the presence of MBs at the interface between the wall of UIAs and surrounding brain tissue. This was validated by the presence of hemosiderin both by direct visualization during microsurgical clipping and immunostaining of aneurysm wall tissue from subjects with sentinel headache [24]. According to Zhang et al., cerebral MBs have been shown to have an independent association with increased risk of aneurysm rupture by approximately 60% [25]. Although QSM has a high specificity in identifying MBs, its post-imaging processing is usually obscured by the presence of bone artifacts (mostly from the clivus and sphenoid clinoid processes) that lie in close anatomical relation with the Circle of Willis. Thus, the strong positive association between aneurysmal wall enhancement and the presence of MBs suggests that this biomarker may detect unstable IAs.

Our study demonstrated that there are statistically significant differences in size, CR_{stalk} measurements, and PHASES scores between stable and unstable UIAs. With these values, we created a receiver operating characteristic curve and identified the best CR_{stalk} cut off with a sensitivity of 82%. However, the specificity was at a lower value of 67%, meaning that one third of patients are at risk of being a false positive. Wang et al. pointed out that when comparing the signal intensities at the neck, body, and dome of IAs, the threshold value would be 0.615 with a sensitivity of 89.5% and specificity of 63.2% [26]. Another study by the same group showed a cutoff of 0.605 using multiple logistic regression analysis with a sensitivity of 90.3% and specificity of 87.9% [27]. These are very similar to our findings from CR_{stalk} measurements comparing the signal intensity of the aneurysmal wall and pituitary stalk.

However, we propose that a lower value of 0.55 can be used as the new threshold for detection.

Based on our results, HR-VWI can be considered as an alternative to MR-QSM when identifying unstable IAs. Larsen et al. has suggested that contrast-enhanced MR vessel wall imaging could detect inflammatory and degenerative changes and enable a clinician to estimate the individual risk of rupture [10]. These results build on the evidence of QSM and HR-VWI as screening tools to detect MB in sentinel headaches. In our previous study, we determined that positive QSM findings strongly suggest MB and that the lack of aneurysmal wall enhancement on HR-VWI can rule out MB with 96.6% accuracy [24]. Having another biomarker for clinicians to detect aneurysmal instability may ultimately lead to expedited treatment and reduced rates of aneurysmal SAH.

5. Limitations

This study is limited by its small sample size. While many patients and aneurysms were recruited, around 54 (31%) had to be excluded primarily due to lack of adequate QSM imaging necessary to confirm the presence or absence of MBs in the aneurysmal wall. Also, this study was conducted within a single center, which limits the generalizability of the results to larger populations. Future multicenter studies with a larger cohort are recommended to confirm these results. This research is not intended to replace other standardized methods of aneurysm detection/assessment but rather to serve as a reliable biomarker of aneurysm instability and risk of rupture.

6. Conclusion

There is a strong positive association between aneurysmal wall enhancement in HR-VWI and MBs detected on QSM sequences. $CR_{stalk} \geq 0.55$ may be used as a complimentary tool to non-contrasted head CT and lumbar puncture in evaluating aneurysmal instability.

Disclosures

None.

References

1. Matouk CC, Mandell DM, Gunel M, et al. Vessel wall magnetic resonance imaging identifies the site of rupture in patients with multiple intracranial aneurysms: Proof of principle. Neurosurgery 72 (2013): 492-496.
2. Lv N, Karmonik C, Chen S, et al. Relationship between aneurysm wall enhancement in vessel wall magnetic resonance imaging and rupture risk of unruptured intracranial aneurysms. Neurosurgery 84 (2019): 385-391.
3. Backes D, Hendrikse J, van der Schaaf I, et al. Determinants of gadolinium-enhancement of the aneurysm wall in unruptured intracranial aneurysms. Neurosurgery 83 (2018): 719-725.
4. Liu P, Qi H, Liu A, et al. Relationship between aneurysm wall enhancement and conventional risk factors in patients with unruptured intracranial aneurysms: A black-blood mri study. Interv Neuroradiol 22 (2016): 501-505.
5. Quan K, Song J, Yang Z, et al. Validation of wall enhancement as a new imaging biomarker of unruptured cerebral aneurysm. Stroke 50 (2019): 1570-1573.
6. Wang GX, Li W, Lei S, et al. Relationships between aneurysmal wall enhancement and conventional risk factors in patients with intracranial aneurysm: A high-resolution mri study. J Neuroradiol 46 (2019): 25-28.

7. Hu P, Yang Q, Wang DD, et al. Wall enhancement on high-resolution magnetic resonance imaging may predict an unsteady state of an intracranial saccular aneurysm. Neuroradiology 58 (2016): 979-985.
8. Shimonaga K, Matsushige T, Ishii D, et al. Clinicopathological insights from vessel wall imaging of unruptured intracranial aneurysms. Stroke 49 (2018): 2516-2519.
9. Hudson JS, Zanaty M, Nakagawa D, et al. Magnetic resonance vessel wall imaging in human intracranial aneurysms. Stroke 50 (2018).
10. Larsen N, von der Brelie C, Trick D, et al. Vessel wall enhancement in unruptured intracranial aneurysms: An indicator for higher risk of rupture? High-resolution mr imaging and correlated histologic findings. AJNR Am J Neuroradiol 39 (2018): 1617-1621.
11. Matsushige T, Shimonaga K, Mizoue T, et al. Focal aneurysm wall enhancement on magnetic resonance imaging indicates intraluminal thrombus and the rupture point. World Neurosurg 127 (2019): 578-584.
12. Vergouwen MDI, Backes D, van der Schaaf IC, et al. Gadolinium enhancement of the aneurysm wall in unruptured intracranial aneurysms is associated with an increased risk of aneurysm instability: A follow-up study. AJNR Am J Neuroradiol 40 (2019): 1112-1116.
13. Gariel F, Ben Hassen W, Boulouis G, et al. Increased wall enhancement during follow-up as a predictor of subsequent aneurysmal growth. Stroke 51 (2020): 1868-1872.
14. Liu C, Li W, Tong KA, et al. Susceptibility-weighted imaging and quantitative susceptibility mapping in the brain. J Magn Reson Imaging 42 (2015): 23-41.
15. Li W, Avram AV, Wu B, et al. Integrated laplacian-based phase unwrapping and background phase removal for quantitative susceptibility mapping. NMR Biomed 27 (2014): 219-227.
16. Fedorov A, Beichel R, Kalpathy-Cramer J, et al. 3d slicer as an image computing platform for the quantitative imaging network. Magn Reson Imaging 30 (2012): 1323-1341.
17. Tan H, Zhang L, Mikati AG, et al. Quantitative susceptibility mapping in cerebral cavernous malformations: Clinical correlations. AJNR Am J Neuroradiol 37 (2016): 1209-1215.
18. Roa JA, Zanaty M, Osorno-Cruz C, et al. Objective quantification of contrast enhancement of unruptured intracranial aneurysms: A high-resolution vessel wall imaging validation study. J Neurosurg (2020): 1-8.
19. Roa JA, Zanaty M, Ishii D, et al. Decreased contrast enhancement on high-resolution vessel wall imaging of unruptured intracranial aneurysms in patients taking aspirin. J Neurosurg (2020): 1-7.
20. Dhar S, Tremmel M, Mocco J, et al. Morphology parameters for intracranial aneurysm rupture risk assessment. Neurosurgery 63 (2008): 185-196.
21. Greving JP, Wermer MJ, Brown RD, et al. Development of the phases score for prediction of risk of rupture of intracranial aneurysms: A pooled analysis of six prospective cohort studies. Lancet Neurol 13 (2014): 59-66.

22. Backes D, Rinkel GJE, Greving JP, et al. Elapss score for prediction of risk of growth of unruptured intracranial aneurysms. Neurology 88 (2017): 1600-1606.
23. Etminan N, Brown RD, Jr., Beseoglu K, et al. The unruptured intracranial aneurysm treatment score: A multidisciplinary consensus. Neurology 85 (2015): 881-889.
24. Ishii D, Nakagawa D, Zanaty M, et al. Quantitative susceptibility mapping and vessel wall imaging as screening tools to detect microbleed in sentinel headache. J Clin Med (2020): 9.
25. Zhang X, Yao ZQ, Karuna T, et al. Cerebral microbleeds could be independently associated with intracranial aneurysm rupture: A cross-sectional population-based study. World Neurosurg 115 (2018): 218-225.
26. Wang GX, Wen L, Lei S, et al. Wall enhancement ratio and partial wall enhancement on mri associated with the rupture of intracranial aneurysms. J Neurointerv Surg 10 (2018): 566-570.
27. Wang GX, Gong MF, Zhang D, et al. Wall enhancement ratio determined by vessel wall mri associated with symptomatic intracranial aneurysms. Eur J Radiol 112 (2019): 88-92.